Rotational Doppler shift of the light transmitted behind a rotating object with rotational symmetries: rotational Doppler shift of the transmitted light

Olivier Emile, Janine Emile, Christian Brousseau, Tangi Le Guennic, Pu Jian, Guillaume Labroille

▶ **To cite this version:**

Olivier Emile, Janine Emile, Christian Brousseau, Tangi Le Guennic, Pu Jian, et al.. Rotational Doppler shift of the light transmitted behind a rotating object with rotational symmetries: rotational Doppler shift of the transmitted light. The European Physical Journal D : Atomic, molecular, optical and plasma physics, 2022, 76 (1), pp.8. 10.1140/epjd/s10053-022-00338-1 . hal-03552800

HAL Id: hal-03552800
https://hal.science/hal-03552800

Submitted on 29 Apr 2022

HAL is a multi-disciplinary open access archive for the deposit and dissemination of scientific research documents, whether they are published or not. The documents may come from teaching and research institutions in France or abroad, or from public or private research centers.

L'archive ouverte pluridisciplinaire **HAL**, est destinée au dépôt et à la diffusion de documents scientifiques de niveau recherche, publiés ou non, émanant des établissements d'enseignement et de recherche français ou étrangers, des laboratoires publics ou privés.

Distributed under a Creative Commons Attribution - NonCommercial 4.0 International License

Eur. Phys. J. D manuscript No.
(will be inserted by the editor)

Rotational Doppler shift of the light transmitted behind a rotating object with rotational symmetries

Rotational Doppler shift of the transmitted light

Olivier Emile[a,1], Janine Emile[2], Christian Brousseau[3], Tangi le Guennic [4], Pu Jian [4], Guillaume Labroille [4]

[1]Université de Rennes 1, Campus de Beaulieu, F-35000 Rennes, France
[2]Université de Rennes 1, CNRS IPR UMR 6251, F-35000 Rennes, France
[3]Université de Rennes 1, CNRS IETR UMR 6164, F-35000 Rennes, France
[4]CAILabs, 38 boulevard Albert 1er, F-35200 Rennes, France
Received: date / Accepted: date

Abstract We investigate both theoretically and experimentally the decomposition of a fundamental Gaussian beam transmitted behind an absorbing propeller-like object. We use a Laguerre Gaussian basis which modes carry orbital angular momentum. The main contributing components correspond to modes having the same rotational symmetry as the object, thus enabling pattern recognition. When the object is rotated, the frequency of the modes of the basis experiences a rotational Doppler shift characterizing the movement, that can be easily detected. Potential applications in target recognition and rotation identification are then considered, including rotational Doppler shifts using microwaves.

1 Introduction

The rotational Doppler effect is rooted in the rotational motion between the source and the observer [1,2]. It is the counter part of the linear Doppler effect for rotating bodies. It potentially shares the same applications for the rotational movement as the linear Doppler effect for the transverse displacement. However, there are two main drawbacks that have, up to now, strongly limited its practical use. First, whereas the linear Doppler can be observed with any kind of beam, the rotational Doppler effect requires the use of special beams carrying either Spin Angular Momentum (SAM) or Orbital Angular Momentum (OAM). Second, and most of all, just as the linear momentum of the wave has to change during wave and object interaction in the case of the linear Doppler effect, the total angular momentum (SAM+OAM) of the wave has also to change during wave and rotating body interaction [2,3] for the rotational Doppler effect. In optics, its implementation has thus been restricted either i) to the transmission through specific rotating elements such as spiral wave plates or dove prisms [4,5], or ii) to the scattering by rough surfaces [6–8] or from ion-acoustic vortices in laser plasma [9], or iii) to the reflection on phase conjugated mirrors [10,11], metasurfaces and helicoidal reflectors [12–14] or prisms [15].

Very recently, a rotational Doppler effect has been experimentally reported in the decomposition into Laguerre Gaussian (LG) modes of the transmitted light from a fundamental beam through a specific object with π rotational symmetry, more precisely, a rotating rod [16]. Then the question arises whether i) identification of object and ii) rotational Doppler effect could be theoretically predicted and experimentally observed for other kind of objects, whatever their rotational symmetry. The aim of this article is thus to deeply investigate both theoretically and experimentally the transmitted light through a modeled propeller with several blades and look for frequency shifts in the light decomposition in LG modes as the object is rotated.

The article is organized as followed. After this introduction, we briefly present the experimental set-up used to observe the rotational Doppler effect (section 2). We then calculate the decomposition of the transmitted light on a LG basis after a modelled propeller (section 3). The experimental results concerning the decomposition of the transmitted light and on the rotational Doppler effect are presented in section 4. We finally discuss these results in the last section (section 5),

[a]emile@univ-rennes1.fr

Accepted manuscript / Final version

together with potential applications, before reaching a conclusion.

2 Experimental set-up

The experimental set-up has been described previously [16]. Nevertheless we here recall its main characteristics. It is displayed in figure 1. The fundamental beam of an infrared laser (CEFL, Keopsys, $\lambda = 1.55$ μm, connected to a single mode fibre SMF-28 and a collimating lens) is mode-matched to the fundamental mode of a commercially available space division multiplexing unit based on Multi-Plane Light Conversion (MPLC) [17, 18]. Briefly, on a theoretical point of view, any unitary spatial transform can be implemented by a succession of transverse phase profiles separated by free space propagation for optical Fourier transforms. The MPLC cavity is formed by one mirror and one reflective phase plate, performing the successive phase profiles and optical transforms, to realize a given unitary spatial transform, with low optical losses and high modal selectivity. The 400 μm-waist of the MPLC is located 3 mm after the entrance window. Although the MPLC has been here configured to multiplex or demultiplex Hermite-Gaussian modes (HG), it can address any spatial mode profile, in particular LG beams, with high reliability.

Note that we are working with an infrared radiation that is eye-safe. There is thus no risk in using it in free space propagation, especially in public areas. Besides, there is a lot of commercially available fibre connected elements originating from telecommunications systems that could be used to either couple, modulate, analyze or attenuate signals at this wavelength. Nevertheless, the optics of the MPLC can be adapted whatever the wavelength.

Since the multiplex/demultiplex operation of the MPLC corresponds to HG modes that have cartesian symmetry, we insert a $\pi/2$ converter based on cylindrical lenses before the MPLC unit, to convert LG beams into HG beams [19–21]. Then, the association of a mode converter and the spatial multiplexer demultiplexes into LG beams that have cylindrical symmetry. We have checked by sending light backward in each output of the MPLC that the emerging light indeed corresponds to LG beams. For this purpose, we used the double slit experiment. Briefly, compared with the usual straight line of the interference fringes of the Young double slit experiment for a plane wave, the interference pattern for OAM beams is twisted by an integer number order corresponding to the topological charge of the beam [22].

We insert the rotating object just before the mode-matching lens (see Fig. 1). It is a drawing of one or several regularly spaced angular areas that mimic a propeller which have been printed on a transparency (see Fig. 2). It is fixed on a homemade hollow shaft driven by a belt and a motor. We take great care to align the centre of symmetry of the inserted object both with the rotation axis and with the optical axis of the experimental device.

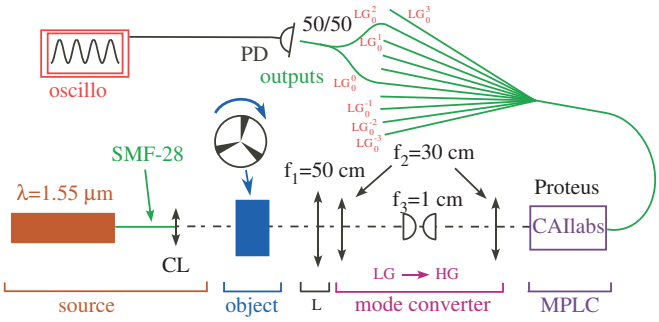

Fig. 1 Experimental set-up. Continuous wave laser source: $\lambda = 1.55$ μm. CL: collimating lens at the output of the fibre to collimate the laser. L: $f_1 = 50$ cm : mode matching lens. $f_2 = 30$ cm: focussing lenses; distance between them 60 cm. $f_3 = 1$ cm: cylindrical lenses acting as a $\pi/2$ converter; distance between them 1.41 cm. MPLC: spatial multiplexer. PD: photodiode. 50/50: coupler with a 50/50 intensity repartition. Oscillo: oscilloscope.

As the rotating object is interposed, the light transmission is not mode matched to the fundamental beam anymore. We decompose it into LG modes with the help of the MPLC and the $\pi/2$ converter. The output of each demultiplexed mode is coupled to an optical fibre. It can then be plugged to a photodiode to register the intensity in order to investigate the decomposition of the transmitted beam in LG modes. Alternatively, the fibres could be coupled to one another or to a reference beam (called hereafter the reference signal) originating from the laser source, thanks to optical fibre couplers. We can then study the beat frequencies between the modes and thus look for frequency shifts.

3 Theoretical considerations

3.1 Light decomposition in the LG basis

Let us first investigate, from a theoretical point of view, the decomposition of the transmitted light behind an object in the LG basis. We denote the LG beams LG_p^ℓ, where p is the radial order and ℓ is the azimuthal order or topological charge [23]. The rotating objects are displayed in Fig. 2. They mimic propellers with one, two, or three blades. Their diameter is 1.5 cm. Such objects have $2\pi/n$ symmetry, with $n = 1, 2, 3$ respectively, depending on the number of blades. The light transmission $f(\theta)$, θ being the azimuthal angle (with counter

Accepted manuscript / Final version

clockwise positive convention), behind such objects can be written as

$$f(\theta) = 1 \quad \text{for} \quad \theta_0 + \frac{2\pi m}{n} \leq \theta \leq -\theta_0 + \frac{2\pi(m+1)}{n} \\ f(\theta) = 0 \text{ otherwise} \tag{1}$$

m being an integer varying between 0 and $n-1$, and θ_0 being half of the dark opening angle ($\theta_0 = \pi/12$ in our situation). We here omit diffraction phenomena.

The electric field of the LG_p^ℓ modes can be written as [23–25]

$$E_p^\ell(r,\theta,z) = A_p^\ell(r,z) e^{i\frac{kr^2}{2R(z)}} e^{i\ell\theta} e^{-i\varphi_p^\ell(z)} e^{i(kz-\omega t)} \tag{2}$$

with

$$A_p^\ell(r,z) = \sqrt{\frac{(2p)!}{\pi(p+|\ell|)!}} \frac{\sqrt{P_0}}{w(z)} (\frac{r\sqrt{2}}{w(z)})^{|\ell|} L_p^{|\ell|}(\frac{2r^2}{w^2(z)}) e^{-\frac{r^2}{w^2(z)}}$$

(r,θ,z) are the cylindrical coordinates, ω is the pulsation of the electromagnetic wave and k is its wavevector. P_0 is the optical power, $w(z)$ is the waist of the beam at the z position, $R(z)$ is its radius of curvature. $\varphi_p^\ell(z) = (2p+|\ell|+1)\arctan(\frac{z}{z_R})$ is the Gouy phase and z_R is the Rayleigh zone [26]. We assume here that we are far from the Rayleigh zone and we thus neglect this Gouy phase. $L_p^{|\ell|}$ is the Laguerre polynomial of order n. It equals to

$$L_p^{|\ell|}(x) = \frac{x^{-|\ell|}e^x}{p!} \frac{d^p}{dx^p}(e^{-x}x^{p+|\ell|}) \tag{3}$$

Let us have a look to the first three polynomials.

- For $p=0$, $L_0^{|\ell|}(x) = 1$
- For $p=1$, $L_p^{|\ell|}(x) = -x + (|\ell|+1)$
- For $p=2$, $L_2^{|\ell|}(x) = \frac{1}{2}x^2 - (|\ell|+2)x + \frac{1}{2}(|\ell|+2)(|\ell|+1)$

In order to decompose the transmitted field in a LG basis, one has to calculate the overlap between this transmitted field and the LG_p^ℓ modes. It writes

$$I_p^\ell(z) = \int_0^\infty r dr \int_0^{2\pi} E_p^\ell(r,\theta,z)^* E_1(r,\theta,z) d\theta \tag{4}$$

where $(^*)$ denotes the complex conjugate of the LG mode and $E_1(r,\theta,z)$ is the transmitted field at position z . It is the fundamental mode times the transfer function $f(\theta)$ of the occulting object. It equals

$$E_1(r,\theta,z) = \sqrt{\frac{2}{\pi}} \frac{1}{w} e^{-\frac{r^2}{w^2}} f(\theta) e^{i\frac{kr^2}{2R(z)}} e^{i(kz-\omega t)} \tag{5}$$

where we have normalized the incident power to unity ($P_0 = 1$). Since without the rotating object, the incident beam is mode matched to the fundamental beam, the two fields in Eq. 4 are evaluated at the same z position. They have the same waist and the same phase factor due to propagation and time dependence. These phase terms thus cancel in the integral calculus. There is thus no dependence on the position of Eq. 4.

The integral in Eq. 4 could be decomposed in a radial part

$$K_p^\ell = \frac{1}{\pi\sqrt{2}} \sqrt{\frac{(2p)!}{(p+|\ell|)!}} \int_0^\infty u^{|\ell|} L_p^{|\ell|}(u) e^{-u^2} u du \tag{6}$$

where $u = \dfrac{2r^2}{w^2}$, and an angular part that doesn't depend on p

$$I^\ell = \int_0^{2\pi} f(\theta) e^{-i\ell\theta} d\theta = \sum_{m=0}^{n-1} \int_{\theta_0+\frac{2\pi m}{n}}^{-\theta_0+\frac{2\pi(m+1)}{n}} e^{-i\ell\theta} d\theta \tag{7}$$

Let us first focus on this angular part. There are two very different cases. First, for $\ell = 0$, i.e. for the case corresponding to the fundamental mode, the integral writes

$$I^0 = \sum_{m=0}^{n-1} (-\theta_0 + \frac{2\pi(m+1)}{n} - \theta_0 - \frac{2\pi m}{n}) = 2\pi - 2n\theta_0 \tag{8}$$

It equals 2π when $n = 0$, i.e. when there is no occulting object. Second, for $\ell \neq 0$, the integral equals

$$I^\ell = \frac{2}{\ell} \sin(-\ell(-\theta_0 + \frac{\pi}{n})) e^{-i\ell\frac{\pi}{n}} \sum_{m=0}^{n-1} e^{-2im\ell\frac{\pi}{n}} \tag{9}$$

- If ℓ is a multiple of n ($\ell = n \times q$), then

$$I^\ell = \frac{2n}{\ell} \sin(\ell\theta_0) \tag{10}$$

- $I^\ell = 0$ otherwise.

It means that if the topological charge ℓ is not a multiple of n, there is no component of the transmitted beam on the LG_p^ℓ mode, whatever the value of p. This result could also have been found using symmetry arguments. If the object (and also the transmitted light) and the LG_p^ℓ beam have not the same rotational symmetry, then, the overlap between the transmitted beam and the LG_p^ℓ beam is zero.

Concerning the radial part (Eq. 6), one can find an analytical expression and then evaluate it. For example

$$K_0^0 = \frac{1}{\pi} \int_0^\infty e^{-u^2} u du = \frac{1}{2\pi} \tag{11}$$

Thus $K_0^0 I^0 = 1$ for $n = 0$, which corresponds to the mode matching condition with the fundamental mode in the absence of any occulting object. The result of the theoretical decomposition of the transmitted beam on the LG basis is displayed in Fig. 2, where we have plotted the intensity of the mode (square of the modulus of I^ℓ) for different values of ℓ. Note that the scale

Accepted manuscript / Final version

is different for the LG_0^0 mode and the other modes, in order to exemplify their contribution. We have chosen an arbitrary value of 8 for the vertical scale that corresponds to the absence of any occulting object for the LG_0^0 mode, in order to compare it with the experimental data (8 mW for the mode matching condition for the LG_0^0 mode).

Fig. 2 evidences that the LG_0^ℓ and the $LG_0^{-\ell}$ have exactly the same contribution as expected from Eq. 10, since only the absolute value of ℓ is taken into account. Besides, apart from the fundamental mode, the dominant modes are the $LG_0^{|\ell|}$ modes where $|\ell|$ corresponds to the rotational symmetry of the occulting object. Since the angular area of the occulting object is small compared with the rest of the object, the main contribution of the transmitted signal remains the LG_0^0 mode. As the occulting area increases (θ_0 increases), the contribution of the fundamental mode decreases regularly (see Eq. 8). The contribution of the other leading modes increases until the dark sector occupies half of the surface and then deceases (see Eq. 10).

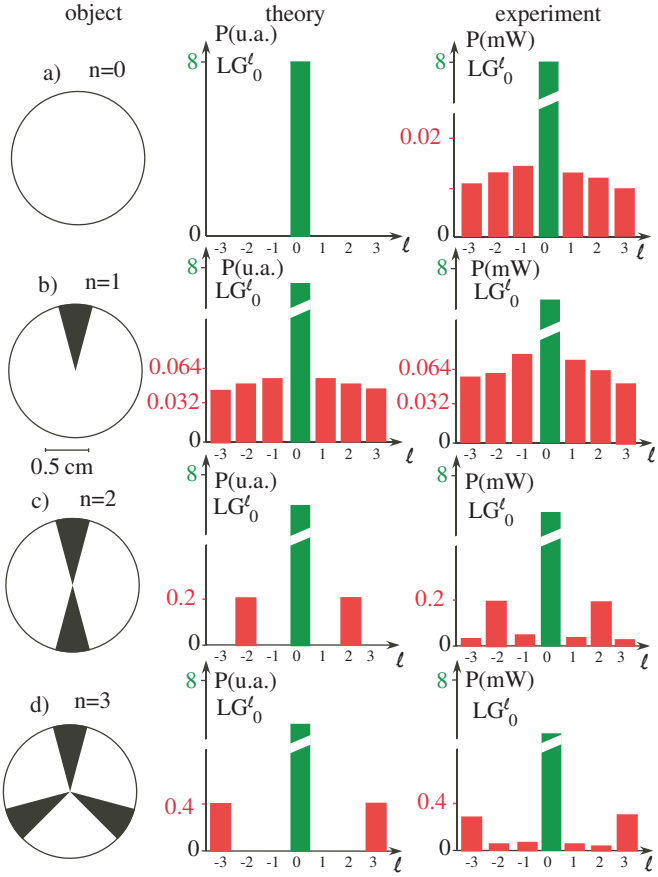

Fig. 2 Shape of the object, theoretical decomposition of the transmitted beam (square of the I^ℓ integral) and experimental decomposition for a $2\pi/n$ symmetry of the rotating object for a) $n = 0$, b) $n = 1$, c) $n = 2$ and d) $n = 3$. Note that the scale is different for the LG_0^0 and the other LG_p^ℓ modes. The scale of the theoretical curves has been adapted to the experimental ones.

3.2 Rotational Doppler shift

The occulting object is now rotated. Let us first consider a given static rotation of an angle θ_r of the object compared with the previous reference situation. The shadow of the transmitted beam is rotated by the same value. This rotation is nothing but a translation of the origin of the angles. Consequently, for a LG beam with a topological charge ℓ that has an azimuthal variation, an extra term $e^{i\ell\theta_r}$ appears in the sum of Eq. 2. It could be factorized. There is thus a phase shift that equals $\ell\theta_r$, in the expression of the field of the LG_p^ℓ. This phase shift depends on the topological charge ℓ and on the angle θ_r. There is no change in the decomposition in the LG basis since Eq. 7 becomes

$$I^\ell = e^{-i\ell\theta_r} \sum_{m=0}^{n-1} \int_{\theta_0+\frac{2\pi m}{n}}^{-\theta_0+\frac{2\pi(m+1)}{n}} e^{-i\ell\theta} d\theta \qquad (12)$$

The square of I^ℓ is unchanged.

As the object is now rotating at a constant angular velocity Ω_r, θ_r can written $\theta_r = \Omega_r t$. Then, the phase shift $\ell\Omega_r t$ could be included in the time dependence ($e^{-i\omega t}$) of the electric field in Eq. 2. It is equivalent to a frequency shift $-\ell\nu_r$ with $\nu_r = \Omega_r/(2\pi)$. This is nothing but a Doppler rotational frequency shift [1,2] proportional to the topological charge times the rotation frequency. The calculations have been carried out with a LG_0^0 incoming mode. Nevertheless the conclusions are still valid with a LG_0^ℓ mode. The $LG_0^{\ell'}$ mode in the decomposition would then be shifted by a $(\ell' - \ell)\nu_r$ value.

It is worth noting that for a positive topological charge of the LG mode, as the object rotates counterclockwise, i.e. in the same sense as the phase rotation of the mode, the frequency of the mode is red shifted (its frequency decreases), whereas for a negative topological charge of the LG mode, the frequency is blue shifted (its frequency increases) also for a counterclockwise rotation. The conclusions are of course reversed for a clockwise rotation. It is analogous to the usual Doppler shift where the frequency is red shifted as the source is moving closer to the detector, and the frequency is blue shifted as the source moves away from the detector.

Accepted manuscript / Final version

4 Experimental results

4.1 Static occulting object

We have first connected the various outputs of the MPLC unit corresponding to LG_0^ℓ with topological charges $\ell = 0, 1, 2, 3$ to a power meter and registered the light power, with or without static objects. This is displayed in Fig. 2. As already mentioned for the theoretical curves, the scale, is different for the central peak ($\ell = 0$), and the other peaks ($\ell \neq 0$). The scales of the theoretical and experimental curves have been adapted to correspond to one another. Fig. 2a shows the intensities for $n = 0$, i.e. when there is no occulting object. It thus corresponds to the injection of the mode from the laser source into the fundamental mode of the MPLC. This injection is rather good with less then 1% of the initial intensity appearing in the other modes than the fundamental one. The source and the detector are correctly mode-matched.

Fig. 2b, c, d display the experimental intensities of the LG_0^ℓ modes for $n = 1, 2, 3$ respectively, i.e. when the object has a 2π, π, or $2\pi/3$ symmetry respectively. It can be noted that the intensities of the peaks with opposite topological charges are almost the same, as expected from the theoretical considerations. In the case of $n = 1$ (2π symmetry, see Fig. 2b) apart from the $\ell = 0$ peak, the dominant peaks correspond to $\ell = \pm 1$ i.e. to the mode having the same symmetry as the rotating object. However the peaks corresponding to $\ell = \pm 2$ and $\ell = \pm 3$ are although present, as expected. The agreement with the theoretical values is rather good. Nevertheless we note that the intensity of the side peaks is little more than expected. It is probably due to that the residual signal on the peaks with non zero topological charge in the absence of any object (mode matching condition) is not negligible compared with the expected signal for a $n = 1$ object.

For a $n = 2$ or $n = 3$ symmetry (Fig. 2c and 2d), only the experimental peaks corresponding to LG beams having the same rotational symmetry as the object have a significant contribution, as expected. The magnitude of the peaks is in good agreement with the expected theoretical values of Fig. 2c and 2d. This shows that the MPLC unit decomposes the transmitted light behind the static occulting object having a given symmetry, into LG modes with a high quality. Besides, the dominant modes in the decomposition (apart the contribution of the fundamental mode) determine the symmetry of the object.

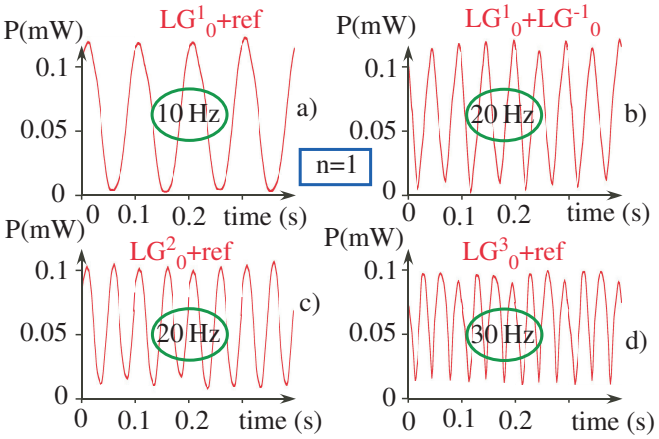

Fig. 3 Beat frequencies for a $\nu_r = 10$ Hz rotation frequency of the object that has a 2π rotational symmetry ($n = 1$), between a) The LG_0^1 mode and the reference signal, b) The LG_0^1 and LG_0^{-1} modes, c) The LG_0^2 mode with the reference signal, d) The LG_0^3 mode with the reference signal. The number circled in red corresponds to the beat frequency.

4.2 Rotating object

Let us now rotate the absorbing object at a given frequency ν_r. We have first checked on a photodiode that there is only a little residual modulation of the intensity of each mode when detected separately. It corresponds to less than 5 % of the total intensity. This residual modulation results probably from a very slight misalignment of the rotation axis with the optical axis. In order to investigate on frequency shifts, we have mixed the output of the MPLC corresponding to a given ℓ value to light originating directly from the laser source, i.e. the reference signal. We have also mixed the outputs of the MPLC with one another.

We show on Fig. 3 the various beat frequencies ν_b for a rotation frequency of the object $\nu_r = 10$ Hz, for an object with a 2π rotational frequency ($n = 1$). There is obviously a strong modulation of the intensity of the coupled outputs, that is due to different frequencies of the mixed beams. Although the experimental data for LG_0^ℓ, with $\ell = -1, -2, -3$ are not shown on Fig. 3, we observe the same modulation signal as for the beat frequency between the reference signal and the $\ell = 1, 2, 3$ modes. For a LG beam with a topological charge $\ell = \pm 1$ (see Fig. 3a), the beat frequency with the reference signal equals $\nu_b = 10$ Hz$= |\ell|\nu_r$. For a $\ell = \pm 2$ topological charge (see Fig. 3c), the beat frequency equals 20 Hz, and for a $\ell = \pm 3$ (see Fig. 3d) the beat frequency equals 30 Hz, in agreement with the $|\ell|\nu_r$ frequency shift. These results are similar to those that have been obtained recently using a spatial light modulator to mimic the image of rotating objects that have $n = 3$ and $n = 5$ rotational symmetry [27].

Accepted manuscript / Final version

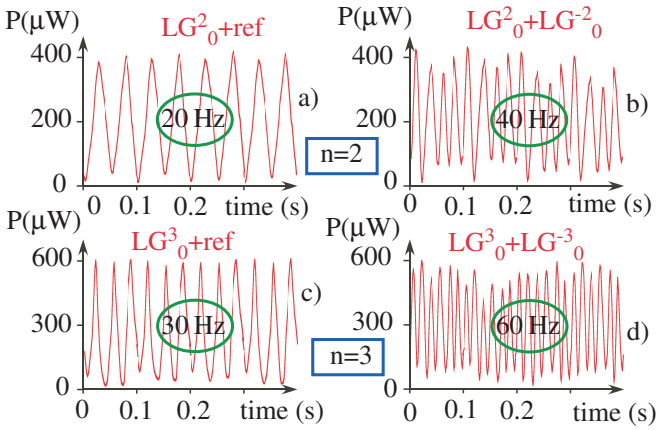

Fig. 4 Beat frequencies for a $\nu_r = 10$ Hz rotation frequency of the object between a) The LG_0^2 mode and the reference signal, b) The LG_0^2 and LG_0^{-2} modes, for an object having a π rotational symmetry ($n = 2$) and c) The LG_0^3 mode with the reference signal, d) The LG_0^3 and LG_0^{-3} modes, for an object having a $2\pi/3$ rotational symmetry ($n = 3$).

These results are consistent with a shift of the LG beam corresponding to the rotational Doppler shift formula. This modulation of the beat signal cannot be attributed to a modulation of the signal of the different outputs alone, since there is only a very small residual modulation on a single output intensity of the MPLC.

For a higher rotational symmetry of the object ($n = 2, 3$), we have also investigated the beat frequencies between the reference signal and the LG beams LG_0^ℓ with a topological charge $\ell = \pm n$. The beat frequency equals $\nu_b = |\ell| \times 10$ Hz$= |\ell|\nu_r$ (see Fig. 4a and b). The beat frequencies with the other LG beams with topological charges that are not multiple of n are negligible. This is consistent with the results found in Fig. 2.

We also observe the same beat frequency when the reference signal is replaced by the output of the MPLC corresponding to the fundamental beam. Besides, when the LG_0^0 is mixed with the reference signal there is no modulation. Obviously the LG_0^0 mode is not shifted and keeps the same frequency. When we couple the output of the MPLC corresponding to LG beams with opposite topological charges, we observe a beat frequency that equals $\nu_b = |\ell| \times 2 \times 10$ Hz$= 2|\ell|\nu_r$. (see Figs. 3b, 4b, 4d). This is also consistent with a shift of the LG beam corresponding to the rotational Doppler shift formula. Moreover, this implies that the outputs of the MPLC corresponding to opposite topological charges ℓ and $-\ell$ are shifted by opposite frequencies: $\ell\nu_r$ and $-\ell\nu_r$.

5 Discussion

5.1 Pattern recognition

We have shown in section 4.1 that the only non-zero components in the decomposition of the transmitted light behind an object having a $2\pi/n$ rotational symmetry are the modes corresponding to LG beams having a topological charge ℓ that is a multiple of the order of the symmetry of the object ($\ell = q \times n$ where q is an integer). Usually, in pattern recognition experiments using OAM, the incident beam carries OAM. One must then choose the incident beam that has the same rotational symmetry as the investigated objet, in order to maximize the signal. In particular, this method has been shown to enhance the sensitivity to phase and amplitude variations [28]. Moreover, correlated OAM states allow the recognition of specific spatial signatures [29]. It is worth noting that such a modal decomposition has also been used to identify the parameters of objects and especially its opening angle [30].

On the contrary here, the incident beam is an ordinary beam. It corresponds to the fundamental mode. It doesn't carry any OAM. We have decomposed the transmitted beam behind an occulting object that has to be identified, on a LG basis. In principle, since the set of the LG modes forms a basis, the transmitted image can thus be precisely and unambiguously reconstructed. Besides, we have shown that for a simple object, the use of only a limited number of LG modes (seven modes in our case) enables to accurately determine the rotational symmetries of the object.

5.2 Rotation detection

However, the most important part of the work reported here is probably about the rotational Doppler effect. Actually, we have measured frequency shifts on the decomposition in a LG basis of the transmission of a usual beam behind a simple rotating object, similar to a propeller, in a bistatic radar configuration. It could also have been observed in reflection, on a simple object, in a monostatic radar configuration. Whereas in nearly all the experiments on the rotational Doppler effect using OAM, the probe beam carries OAM as for pattern recognition experiments, the probe beam is here again the fundamental mode of the laser. There is absolutely nothing special about the incident beam. The variation of the topological charge that is associated with the rotational Doppler effect is observed on the decomposition of the transmitted light on the LG mode basis. Only the modes with non-zero topological charges are

Accepted manuscript / Final version

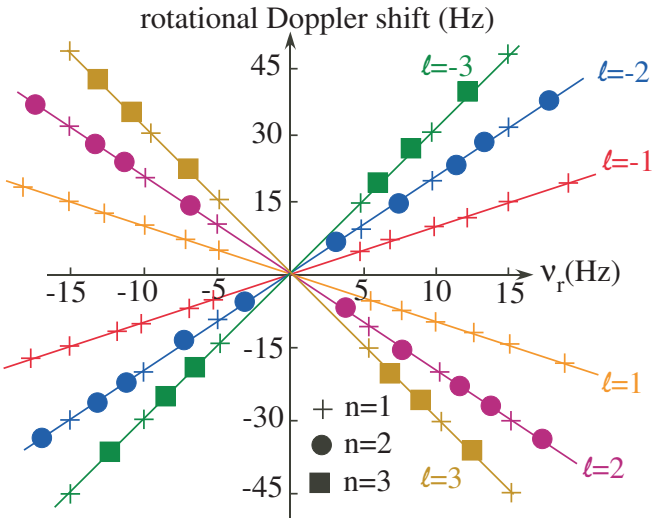

Fig. 5 Experimentally measured rotational Doppler frequency shifts of the LG_0^ℓ modes, with $\ell = -3, -2, -1, 1, 2, 3$ versus the rotation frequency of the object ν_r, for an object having a 2π ($n = 1$) rotational symmetry (cross), a π ($n = 2$) rotational frequency (circle), a $2\pi/3$ rotational symmetry ($n = 3$). The solid lines correspond to the theoretical expected values. The size of the experimental crosses, squares, circles corresponds to the error bars, either horizontal or vertical.

frequency shifted. This shift equals $\nu_b = |\ell|\nu_r$. There is no frequency shift of the fundamental mode.

This frequency shift can be observed for various rotation frequencies of the object (see Fig. 5). For each mode, it varies linearly, as expected from the Doppler shift formula and from the discussion of section 3.2. It is worth noting that the shift for a given mode is independent of the rotational symmetry of the rotating object, as soon as the mode contribution is different from zero. Only the magnitude of the signal is related to the rotational symmetry. This shift only depends on the topological charge of the demultiplexed beam.

Besides, we have shown experimentally that the beat frequency between opposite topological modes is twice the rotation frequency times the absolute value of the topological charge. It shows that the two modes have opposite frequency shifts. Would it be possible to discriminate which mode has the highest frequency and which one has the lowest frequency?

In order to investigate the sign of the rotational Doppler shift, we replace the previous homodyne detection with a heterodyne detection. With two acousto-optic modulators that are fibre connected, we shift the frequency of the reference beam by 70 Hz. We then investigate the beat frequencies with the various modes for different rotation frequencies of the object. We choose the positive sense of rotation of the object as the object rotates clockwise when looking at the object from the detector. We also choose the same convention for the sense of rotation of the phase of the LG beam. We then evidence a beat frequency that is higher when the object and the phase of the mode rotate in opposite direction. The frequency of the mode is blue shifted (it increases), whereas the beat frequency is red shifted (it decreases) when the object and the phase of the mode rotate in the same direction (see Fig. 5). This is in total agreement with the conclusions of section 3.2.

5.3 Potential applications

As in every light/matter interaction, due to the optical radiation pressure effect, the linear velocity of the moving object changes (slightly) during interaction with light, in the case of a linear Doppler shift. Similarly, in the case of a rotational Doppler shift there is also a (slight) change of the rotational velocity of the object. The rotational Doppler shift can thus be measured indirectly, in a dual way. One has to investigate the variation of the rotating velocity itself. Indeed, as pointed out by Padgett [31], the rotational Doppler effect is associated with the power of the applied torque. It must result in a frequency shift and consequently, in a change of the total energy of the field. Due to energy conservation [32], this energy change of the field must be compensated for a change of energy of the object. Unfortunately, in our case, the LG beams with opposite charges have the same weight. After interaction, the energy balance between them has changed. However, the frequency shift of the LG_0^ℓ mode is annihilated by a shift of the frequency of the $LG_0^{-\ell}$ mode with an opposite sign. There is thus no change of energy of the rotating object.

The experiment has been here performed at the infrared wavelength of $\lambda = 1.55$ μm. It could be generalized to any electromagnetic waves depending on the desired applications. In the visible range of the spectrum, for example, OAM waves have been used in underwater ranging [33]. Rotational Doppler experiments such as the ones described here could permit to determine the specificity of underwater rotating objects such as ships or submarines propellers.

However, the most promising part of the rotational Doppler effect seems probably to be in the microwave range of the electromagnetic spectrum. Indeed, on the one hand, radar signals have been used for a long time for a lot of different applications ranging from weather observations [34] to target localization [35], to name a few. On the other hand, OAM radio waves have been demonstrated some years ago [36,37] and are now an exponentially growing area of research. All the applications of the linear Doppler radar for linear veloc-

Accepted manuscript / Final version

ity detection could be directly transposed to rotational Doppler radar for rotating objects. It could be important for example in the identification, classification and rotation measurements, either in propellers or reactors for civil or military applications.

This kind of experiment, dedicated to the observation of the rotational Doppler shift, is not limited to optics and radio wave but could be generalized to the whole electromagnetic spectrum such as X-ray waves [38], and to any wave in general such as electron [39] or acoustic waves [40] where OAM waves have been evidenced. In particular, Doppler radar effects have found a wide range of applications in the acoustic domain. Besides, acoustic rotational effect has been already reported [41,42]. Doppler acoustic imaging and identification could be enriched with rotational frequency information such as the one detailed in this article.

6 Conclusion

To conclude, we have investigated the transmitted light behind an occulting object having a given rotational symmetry. When the object is static, we have evidence, both theoretically and experimentally, that in the decomposition of the transmitted light in a LG basis, only the mode having the same rotational symmetry as the object has a significant contribution. This could easily enable target identification of object with a priori unknown rotational symmetry using a fundamental mode. Besides, when the object rotates, we have isolated a rotational Doppler shift on each LG mode that contributes to the signal. This shift equals the topological charge times the rotational frequency of the object. The modes having the phase rotating in the same sense as the object are red shifted, whereas the other modes are blue shifted.

This work may also find applications in the micro and the nano-world with possible developments towards biology and medicine. Up to now, several experiments have used micro motors to pump or mix tiny amounts of analytes in biofluid media and microfluidics [43]. There is an increasing need to fully characterize such micro motors rotations. A MPLC spatial multiplexer could be coupled to a microscope in order to identify symmetries and follow the micro motor rotation. Analogously, it could also be used to study microswimmer rotation [44]. Such rotation identification could be even pushed further, in particular towards proteins and viruses recognition, and their rotational power which is a key issue [45,46], using OAM and electron microscopes.

Acknowledgements We wish to acknowledge technical support from X. Morvan and J.-R. Thébault.

Authors contributions

All the authors were involved in the preparation of the manuscript and contribute equally. All the authors have read and approved the final manuscript.

References

1. M. Padgett, Nature **443**(7114), 924 (2006)
2. L. Fang, M.J. Padgett, J. Wang, Laser Photon. Rev. **11**(6), 1700183 (2017)
3. M. Mansuripur, in *Optical Trapping and Optical Micromanipulation IX*, vol. 8458 (International Society for Optics and Photonics, 2012), vol. 8458, p. 845805
4. J. Courtial, K. Dholakia, D. Robertson, L. Allen, M. Padgett, Phys. Rev. Lett. **80**(15), 3217 (1998)
5. I. Basistiy, A.Y. Bekshaev, M. Vasnetsov, V. Slyusar, M. Soskin, JETP Lett. **76**(8), 486 (2002)
6. M.P. Lavery, F.C. Speirits, S.M. Barnett, M.J. Padgett, Science **341**(6145), 537 (2013)
7. M.P. Lavery, S.M. Barnett, F.C. Speirits, M.J. Padgett, Optica **1**(1), 1 (2014)
8. A. Ryabtsev, S. Pouya, A. Safaripour, M. Koochesfahani, M. Dantus, Opti. Express **24**(11), 11762 (2016)
9. A.Y. Okulov, Phys. Lett. A **374**(44), 4523 (2010)
10. A.Y. Okulov, J. Phys. B: At. Mol. Opt. Phys. **41**(10), 101001 (2008)
11. A.Y. Okulov, J. Opt. Soc. Am. B **29**(4), 714 (2012)
12. P. Georgi, C. Schlickriede, G. Li, S. Zhang, T. Zentgraf, Optica **4**(8), 1000 (2017)
13. B. Liu, H. Chu, H. Giddens, R. Li, Y. Hao, Sci. Rep. **9**(1), 1 (2019)
14. B. Liu, H. Giddens, Y. Li, Y. He, S.W. Wong, Y. Hao, Opt. Express **28**(3), 3745 (2020)
15. O. Emile, J. Emile, C. Brousseau, Appl. Phys. Lett. **116**(22), 221102 (2020)
16. O. Emile, J. Emile, C. Brousseau, T. le Guennic, P. Jian, G. Labroille, Opt. Lett. **46**(15), 3765 (2021)
17. J.F. Morizur, L. Nicholls, P. Jian, S. Armstrong, N. Treps, B. Hage, M. Hsu, W. Bowen, J. Janousek, H.A. Bachor, J. Opt. Soc. Am. A **27**(11), 2524 (2010)
18. G. Labroille, B. Denolle, P. Jian, P. Genevaux, N. Treps, J.F. Morizur, Opt. Express **22**(13), 15599 (2014)
19. M.W. Beijersbergen, L. Allen, H. Van der Veen, J. Woerdman, Opt. Commun. **96**(1-3), 123 (1993)
20. Y. Torii, N. Shiokawa, T. Hirano, T. Kuga, Y. Shimizu, H. Sasada, Eur. Phys. J. D **1**(3), 239 (1998)
21. J. Courtial, K. O'Holleran, Eur. Phys. J. Special Topics **145**(1), 35 (2007)
22. O. Emile, J. Emile, Appl. Phys. B **117**(1), 487 (2014)
23. L. Allen, M. Padgett, M. Babiker, Prog. Opt. **39**, 291 (1999)
24. G. Molina-Terriza, J.P. Torres, L. Torner, Nat. Physics **3**(5), 305 (2007)
25. A.M. Yao, M.J. Padgett, Adv. Opt. Photon. **3**(2), 161 (2011)
26. A.E. Siegman, *Lasers* (University Science Books, 1986)
27. W. Zhang, J. Gao, D. Zhang, Y. He, T. Xu, R. Fickler, L. Chen, Phys. Rev. Appl. **10**(4), 044014 (2018)
28. L. Torner, J.P. Torres, S. Carrasco, Opt. Express **13**(3), 873 (2005)
29. N. Uribe-Patarroyo, A. Fraine, D.S. Simon, O. Minaeva, A.V. Sergienko, Phys. Rev. Lett. **110**(4), 043601 (2013)

Accepted manuscript / Final version

30. G. Xie, H. Song, Z. Zhao, G. Milione, Y. Ren, C. Liu, R. Zhang, C. Bao, L. Li, Z. Wang, K. Pang, D. Starobudov, B. Lynn, M. Tur, A.E. Willner, Opt. Lett. **42**(21), 4482 (2017)
31. M. Padgett, Proc. Math. Phys. Eng. Sci. **470**(2172), 20140633 (2014)
32. O. Emile, J. Emile, Ann. Phys. **530**(12), 1800111 (2018)
33. A. Jantzi, W. Jemison, A. Laux, L. Mullen, B. Cochenour, Opt. Express **26**(3), 2668 (2018)
34. R.J. Doviak, D.S. Zrnić, *Doppler radar and weather observations* (Courier Corporation, 2006)
35. I. Shames, A.N. Bishop, M. Smith, B.D. Anderson, IEEE Trans. Aerosp. Elect. Syst. **49**(1), 266 (2013)
36. B. Thidé, H. Then, J. Sjöholm, K. Palmer, J. Bergman, T. Carozzi, Y.N. Istomin, N. Ibragimov, R. Khamitova, Phys. Rev. Lett. **99**(8), 087701 (2007)
37. F. Tamburini, E. Mari, B. Thidé, C. Barbieri, F. Romanato, Appl. Phys. Lett. **99**(20), 204102 (2011)
38. J.T. Lee, S. Alexander, S. Kevan, S. Roy, B. McMorran, Nat. Photon. **13**(3), 205 (2019)
39. J. Verbeeck, H. Tian, P. Schattschneider, Nature **467**(7313), 301 (2010)
40. T. Wang, M. Ke, W. Li, Q. Yang, C. Qiu, Z. Liu, Appl. Phys. Lett. **109**(12), 123506 (2016)
41. K. Skeldon, C. Wilson, M. Edgar, M. Padgett, New J. Phys. **10**(1), 013018 (2008)
42. G.M. Gibson, E. Toninelli, S.A. Horsley, G.C. Spalding, E. Hendry, D.B. Phillips, M.J. Padgett, Proc. Natl. Acad. Sci. **115**(15), 3800 (2018)
43. F. Wu, B.G. Van Schie, J.E. Keymer, C. Dekker, Nat. Nanotech. **10**(8), 719 (2015)
44. G. Patil, A. Ghosh, Front. Phys. **8**, 656 (2021)
45. S.D. Karlen, H. Reyes, R. Taylor, S.I. Khan, M.F. Hawthorne, M.A. Garcia-Garibay, Proc. Nat. Acad. Sci. **107**(34), 14973 (2010)
46. J.C. Sinclair, K.M. Davies, C. Vénien-Bryan, M.E. Noble, Nat. Nanotech. **6**(9), 558 (2011)

Accepted manuscript / Final version